

Simultaneous Current Density and Contact Temperature Calculation in a Turbine Generator Exciter Coupling Using FEM

Abstract. A combined simultaneous calculation method for electrical contacts is presented based on a finite element analysis of both the current density distribution as well as the heat flow distribution. For an exact prediction of local hotspots special attention is put on the transition conditions at the joints where current and heat transfer with defined transfer coefficients takes place and temperature and electrical potential face a discontinuity. The conditions for the maximum temperature to be expected at a thermo-electrical contact are derived by an analytical consideration.

Streszczenie. Przedstawiono łączoną metodę obliczeniową dla elektrycznych styków, opartą na analizie metodą elementów skończonych zarówno rozkładu gęstości prądu, jak i przepływu ciepła. W celu dokładnego przewidywania lokalnych przegrzań szczególną uwagę zwrócono na warunki przejścia na złączach, gdzie następuje przekazywanie prądu i ciepła z określonymi współczynnikami przenikania, a temperatura i elektryczny potencjał są nieciągłe. Na drodze analitycznych rozważań wyprowadzono warunki dla maksymalnej temperatury oczekiwanej na termo-elektrycznym styku. (Jednoczesne sprzężone obliczanie gęstości prądu i temperatury styku we wzbudniku turbogeneratora z wykorzystaniem MES).

Keywords: thermo-electrical coupling, FEM, contact temperature, temperature and potential discontinuity

Słowa kluczowe: sprzężenie ciepło-elektryczne, MES, temperatura kontaktowa, temperaturowa i potencjalna nieciągłość.

Introduction

Manufacturers of electrical machines are obliged to keep temperature limits for insulation materials as well as for electrical joints. The temperature at a screwed silver plated contact surface e.g. may not exceed 115 °C [1].

In the case presented a special service modified axial lead connection of an exciter and a generator rotor has to be investigated. The problem is that a newly build generator rotor and a new exciter rotor have to be coupled together as well as with either old counterpart. As a proposed solution the old conical threads in the old exciter rotor would be machined off and replaced by a cylindrical thread, in which an interface bushing is screwed for connection with the new form cylindrical bolts. The inner surface of the interface bushing electrically connects to the bolt via three lamella belts. Fig. 1 shows a view on the exciter coupling.

For this arrangement the question has to be answered whether the additional contact surface in close vicinity to the central insulation layer is thermally admissible or causes too much heat together with the contact lamella belts.

A simultaneous electrical and thermal FEM calculation is carried out to identify and localize existing hot spots since the electrical current density distribution directly influences the temperature distribution via the losses.

Description of the model

The conductive path consists of three parts in electrical and thermal coupling. One is the axial lead itself, which in the electrical model is domain $V_{e,3}$. The other is the adapter threaded bushing, domain $V_{e,2}$. In this the third part – a cylindrical bolt – is inserted, domain $V_{e,1}$.

As shown in Fig. 2 there are four areal electrical contacts in the model. One is the outer thread of the interface bushing in contact to the axial lead, boundary $A_{e,2,3}$. The others are the three contact lamella belts, boundary $A_{e,1,2}$.

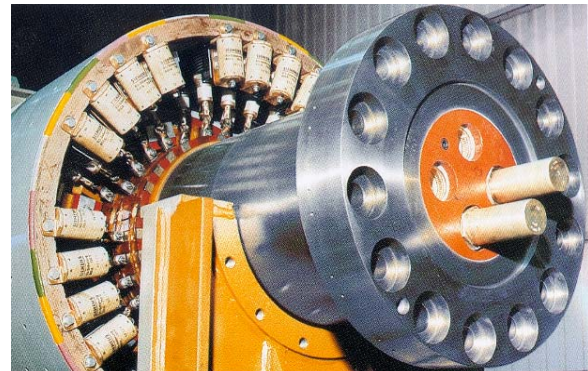


Fig. 1. View on axial lead and exciter coupling.

The thermal model also consists of three domains with only slight differences to the electrical one: Domain $V_{th,3}$ in addition to the axial lead includes the insulation layers, the shaft and the coupling flange, whereas $V_{th,2}$ and $V_{th,1}$ are identical to their electrical pendants. The transition area $A_{th,1,2}$ includes the three lamella belts as well as the spaces between them, where in contrast to electrical current heat transfer is given by conduction through a thin air layer and radiation. $A_{th,2,3}$ is identical to $A_{e,2,3}$.

Owing to symmetry only a quarter of the arrangement has to be modelled including half of the central insulation wall between the positive and the negative lead.

Governing equations

GetDP [2] is used for the treatment of the problem. The electric potential ϕ in case of dc-current density distributions in bulks with conductivity γ is given in its weak formulation with the associated potential test function ϕ .

$$(1) \quad \iiint_V \gamma \operatorname{grad} \phi \cdot \operatorname{grad} \phi \, dV - \iint_{\partial V} \gamma \operatorname{grad} \phi \cdot \vec{n} \, da = 0$$

From the ohmic losses a volumetric loss density p_V results given by the conductivity γ and the current density J :

$$(2) \quad p_V = \frac{J^2}{\gamma} = \gamma \cdot (\text{grad } \varphi)^2$$

Eqn. (1) and (2) are set up and evaluated for the three domains separately. The boundary integrals are used to incorporate the transition conditions as well as the current boundary condition on the front face of the cylindrical bolt.

Eqn. (2) is besides the temperature boundary conditions the excitation of the thermal problem which is analogous to the electrical one:

$$(3) \quad \begin{aligned} & \iiint_{V_{th,i}} \lambda \text{grad } \vartheta \cdot \text{grad } \theta \, dV - \iint_{\partial V} \lambda \text{grad } \vartheta \cdot \theta \vec{n} \, da \\ & - \iiint_V p_V \cdot \theta \, dV = 0 \end{aligned}$$

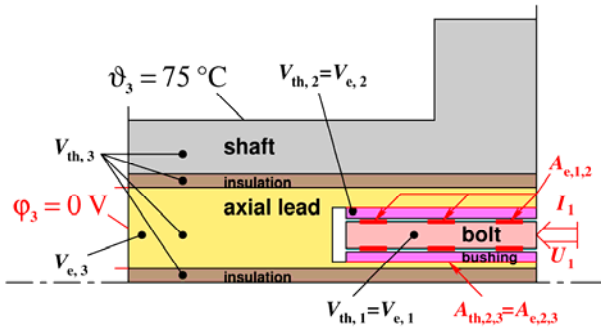


Fig.2. Schematic representation of model with domains, transition areas and external boundary conditions.

Here, ϑ denotes the temperature and λ the thermal conductivity. θ is the corresponding test function. This equation is also set up separately for the three thermal domains.

For the three coupled domains six different function spaces are defined, one for the electrical potential and one for the temperature in each domain. By the definition of different function spaces for each domain the geometrically identical nodes on the surfaces in contact can take two different values of φ and ϑ like in [3] for ϑ .

The transfer conditions given by

$$(4) \quad J_{n,1} = J_{n,2} = -\gamma \text{grad } \varphi \cdot \vec{n} = g_A (\varphi_1 - \varphi_2)$$

for electrical joints and

$$(5) \quad \dot{q}_{n,1} = \dot{q}_{n,2} = -\lambda \text{grad } \vartheta \cdot \vec{n} = \alpha (\vartheta_1 - \vartheta_2)$$

for heat transfer are incorporated into the weak formulation by the surface integrals in (1) and (3). Here, g_A denotes the surface transfer conductivity in S/m^2 and α the heat transfer coefficient in $W/(m^2K)$. The relation between a given contact resistance R_C and the surface transfer conductivity g_A is given by the contact area A_C as follows assuming a uniform distribution of g_A :

$$(6) \quad R_C = \frac{1}{g_A \cdot A_C}$$

The additional heat generated in electrical contacts is described by a surface loss density p_A in the contact area.

$$(7) \quad p_A = \frac{R_C \cdot I^2}{A_C} = R_C A_C J_n^2 = \frac{J_n^2}{g_A} = g_A (\varphi_1 - \varphi_2)^2$$

This loss density symmetrically distributes to the two adjacent domains and is incorporated in (3) by a surface integral.

Arranging all equations in one overall weak formulation with the coupled domains and function spaces the thermal problem can be described by (9), on which Galerkin's method for discretization is applied. The expressions in (9) arise from Poisson's equations for the temperature fields including the Joule heat entries in the domains as well as the contact areas and the coupling terms.

A similar formulation can be established for the electrical problem, which has to be solved in advance in order to obtain the potential distributions $\varphi_{1...3}$ from which the loss densities are calculated in (9). However, as a difference to the thermal problem the function space in domain $V_{e,1}$ has to be constrained in a way that the condition

$$(8) \quad I_1 = - \iint_{A_{\text{bolt,in}}} \gamma \text{grad } \varphi_1 \cdot \vec{n} \, da$$

for a given current I_1 with a floating potential U_1 on the right hand side input surface of the bolt in Fig. 2 can be fulfilled.

An iterative adaption of the electrical conductivity depending on the temperature is possible in principle but is not applied here. Instead, constant values not depending on the temperature are taken.

$$(9) \quad \begin{aligned} & \iiint_{V_{e,1}} \lambda_1 \text{grad } \vartheta_1 \cdot \text{grad } \theta_1 \, dV - \iint_{V_{e,1}} \gamma_1 \cdot (\text{grad } \varphi_1)^2 \cdot \theta_1 \, dV \\ & - \iint_{A_{e,1,2}} \frac{g_{A,1,2}}{2} (\varphi_1 - \varphi_2)^2 \theta_1 \, da \\ & + \iiint_{V_{e,2}} \lambda_2 \text{grad } \vartheta_2 \cdot \text{grad } \theta_2 \, dV - \iint_{V_{e,2}} \gamma_2 \cdot (\text{grad } \varphi_2)^2 \cdot \theta_2 \, dV \\ & - \iint_{A_{e,1,2}} \frac{g_{A,1,2}}{2} (\varphi_2 - \varphi_1)^2 \theta_2 \, da - \iint_{A_{e,2,3}} \frac{g_{A,2,3}}{2} (\varphi_2 - \varphi_3)^2 \theta_2 \, da \\ & - \iint_{A_{e,1,2}} \alpha_{1,2} \vartheta_1 \theta_2 \, da + \iint_{A_{e,1,2}} \alpha_{1,2} \vartheta_2 \theta_2 \, da \\ & - \iint_{A_{e,1,2}} \alpha_{1,2} \vartheta_2 \theta_1 \, da + \iint_{A_{e,1,2}} \alpha_{1,2} \vartheta_1 \theta_1 \, da \\ & + \iiint_{V_{th,3}} \lambda_3 \text{grad } \vartheta_3 \cdot \text{grad } \theta_3 \, dV - \iint_{V_{e,3}} \gamma_3 \cdot (\text{grad } \varphi_3)^2 \cdot \theta_3 \, dV \\ & - \iint_{A_{e,2,3}} \frac{g_{A,2,3}}{2} (\varphi_3 - \varphi_2)^2 \theta_3 \, da \\ & - \iint_{A_{th,2,3}} \alpha_{2,3} \vartheta_2 \theta_3 \, da + \iint_{A_{th,2,3}} \alpha_{2,3} \vartheta_3 \theta_3 \, da \\ & - \iint_{A_{th,2,3}} \alpha_{2,3} \vartheta_3 \theta_2 \, da + \iint_{A_{th,2,3}} \alpha_{2,3} \vartheta_2 \theta_2 \, da = 0 \end{aligned}$$

Analytical considerations on a thin layer model

The situation in an electro-thermal contact can be analysed using a simple three layer model as shown in Fig. 3. The boundary conditions on the intermediate layer are given by a left hand side temperature value ϑ_l and a right hand side value ϑ_r . The intermediate layer with a thickness d and a thermal conductivity λ is also affected by a volumetric loss density p_V . The heat transfer coefficient is

given by $\alpha = \lambda / d$ and the relation between volumetric loss density and the surface loss density is $p_A = p_V d$.

For the intermediate layer the thermal version of Poisson's equation has to be solved for the one-dimensional case as shown in (10) and (11).

$$(10) \quad \text{div}(-\lambda \text{grad } \vartheta) = p_V = -\lambda \frac{d^2 \vartheta}{dx^2}$$

$$(11) \quad \vartheta(x) = -\frac{p_V}{2\lambda} \cdot x^2 + C_1 x + C_0$$

The constants C_0 and C_1 are given by the boundary conditions as follows:

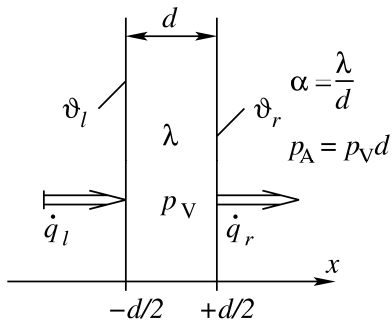


Fig.3. Intermediate layer model for electro-thermal contact situation.

$$(12) \quad \vartheta_l = \vartheta\left(-\frac{d}{2}\right) = -\frac{p_V}{2\lambda} \cdot \frac{d^2}{4} - C_1 \frac{d}{2} + C_0$$

$$(13) \quad \vartheta_r = \vartheta\left(+\frac{d}{2}\right) = -\frac{p_V}{2\lambda} \cdot \frac{d^2}{4} + C_1 \frac{d}{2} + C_0$$

The constants are given by the average temperature decline and the average temperature as shown in (14):

$$(14) \quad C_1 = -\frac{\vartheta_l - \vartheta_r}{d}, \quad C_0 = \frac{\vartheta_l + \vartheta_r}{2} + \frac{p_V}{2\lambda} \cdot \frac{d^2}{4}$$

Thus, the final solution including the assumed boundary temperatures is:

$$(15) \quad \vartheta(x) = -\frac{p_V}{2\lambda} \cdot \left(x^2 - \frac{d^2}{4}\right) - \frac{\vartheta_l - \vartheta_r}{d} x + \frac{\vartheta_l + \vartheta_r}{2}$$

The temperature gradient inside the intermediate layer is:

$$(16) \quad \dot{\vartheta}(x) = -\frac{p_V}{\lambda} \cdot x - \frac{\vartheta_l - \vartheta_r}{d}$$

From this, the heat flow densities on the left hand side and on the right hand side can be calculated by taking (16) at $\pm d/2$ and multiplication with the thermal conductivity:

$$(17) \quad \begin{aligned} \dot{q}_l &= -\lambda \dot{\vartheta}\Big|_{x=-d/2} = -\frac{p_V}{2} \cdot d + \lambda \frac{\vartheta_l - \vartheta_r}{d} = \\ &= -\frac{p_A}{2} + \alpha(\vartheta_l - \vartheta_r) \end{aligned}$$

$$(18) \quad \begin{aligned} \dot{q}_r &= -\lambda \dot{\vartheta}\Big|_{x=d/2} = \frac{p_V}{2} \cdot d + \lambda \frac{\vartheta_l - \vartheta_r}{d} = \\ &= \frac{p_A}{2} + \alpha(\vartheta_l - \vartheta_r) \end{aligned}$$

The results (17) and (18) clearly show that the resultant heat flow densities consist of the internally generated contribution which is symmetrically distributed on both boundaries and the heat transfer component given by the temperature difference and the heat transfer coefficient. This is just the way thin layers are incorporated in (9) as contact surfaces.

Another crucial point which is the maximum temperature in a contact can also be answered by the thin layer model:

If the zero crossing of (16) lies within the interval $[-d/2, d/2]$ then the maximum temperature is given in the contact layer.

$$(19) \quad \dot{\vartheta}(x) = -\frac{p_V}{\lambda} \cdot x - \frac{\vartheta_l - \vartheta_r}{d} = 0$$

The condition results in a dependence of the temperature difference on the surface loss density and the heat transfer coefficient shown in (20) and (21).

$$(20) \quad \left| \frac{x}{d} \right| = \frac{\alpha}{p_A} |\vartheta_l - \vartheta_r| \leq \frac{1}{2}$$

$$(21) \quad |\vartheta_l - \vartheta_r| \leq \frac{p_A}{2\alpha}$$

If (21) holds, the maximum temperature can be calculated by inserting the result from (20) in (15):

$$(22) \quad \begin{aligned} \vartheta_{\max} &= -\frac{p_A}{2\alpha} \cdot \left(\left(\frac{x}{d} \right)^2 - \frac{1}{4} \right) - (\vartheta_l - \vartheta_r) \frac{x}{d} + \frac{\vartheta_l + \vartheta_r}{2} = \\ &= \frac{\alpha}{2p_A} (\vartheta_l - \vartheta_r)^2 + \frac{p_A}{8\alpha} + \frac{\vartheta_l + \vartheta_r}{2} \end{aligned}$$

Otherwise the maximum temperature is either ϑ_l or ϑ_r .

For a junction 1, 2 this finally results in the following cases, where the surface loss density is expressed by the electric potential difference and the contact transfer conductivity:

$$(23) \quad \vartheta_{1,2,\max} = \begin{cases} \frac{\alpha (\vartheta_1 - \vartheta_2)^2}{2g_A (\varphi_1 - \varphi_2)^2} + \frac{g_A}{8\alpha} (\varphi_1 - \varphi_2)^2 + \frac{1}{2} (\vartheta_1 + \vartheta_2), \\ \quad \text{if } |\vartheta_1 - \vartheta_2| \leq \frac{g_A}{2\alpha} (\varphi_1 - \varphi_2)^2; \\ \max(\vartheta_1, \vartheta_2), \quad \text{if } |\vartheta_1 - \vartheta_2| > \frac{g_A}{2\alpha} (\varphi_1 - \varphi_2)^2 \end{cases}$$

Chosen parameters of the model

Crucial parameters of the model are the heat transfer coefficients, the surface current transfer conductivities as well as the volumetric conductivities for heat flow and electric current.

The thermal conductivity of the insulation materials is $\lambda_{\text{iso}} = 0.25 \text{ W/(mK)}$. For the metallic structures of the current path $\lambda_{\text{cond}} = 250 \text{ W/(mK)}$ is estimated. The alloys are somewhat different from pure copper. That is also the reason, why the electrical conductivities of bolt, bushing and axial lead differ from copper: $\gamma_{\text{bolt}} = 45 \text{ MS/m}$, $\gamma_{\text{bush}} = 43 \text{ MS/m}$ and $\gamma_{\text{lead}} = 50 \text{ MS/m}$. The thermal conductivity of the shaft steel is $\lambda_{\text{shaft}} = 36 \text{ W/(mK)}$.

Special attention has to be paid to the surface modelling of the contact lamella belts and the outer bushing thread. For one lamella belt a voltage drop of 20 mV is given by the manufacturer. Assuming this voltage drop occurs at maximum admissible current of 1764 A one can calculate a

resistance of $R_{\text{belt}} = 20 \text{ mV} / 1764 \text{ A} = 11.338 \mu\Omega$ or conductance $G_{\text{belt}} = 1/R_{\text{belt}} \approx 88.2 \text{ kS}$. Distributed on a cylindrical ring with 50 mm diameter and 10 mm width this results in

$$(24) \quad g_{A,\text{belt}} = \frac{G_{\text{belt}}}{A_C} = \frac{88.2 \text{ kS}}{10 \text{ mm} \cdot 50 \text{ mm} \cdot \pi} \approx 56.15 \frac{\text{MS}}{\text{m}^2}$$

For the heat transfer condition in the lamella belt the thermal conductance of a single lamella can be estimated by consideration of the heat path through the lamella. With a length of the heat path of $l = 10 \text{ mm}$, a width of $0.4 \text{ mm} \cdot 2 \cdot \pi = 2.513 \text{ mm}$, a thickness of 0.2 mm and a thermal conductivity of 150 W/(mK) for one half of a lamella the following thermal conductance results:

$$(25) \quad \lambda = \lambda \frac{wt}{l} = 15 \cdot 2.513 \cdot 0.0002 \frac{\text{W}}{\text{K}} \approx 7.54 \cdot 10^{-3} \frac{\text{W}}{\text{K}}$$

For a full lamella this value doubles. With 63 lamellae on the perimeter the total thermal conductance becomes 0.95 W/K . Distributed on the cylindrical surface of the whole belt, an equivalent heat transfer coefficient of

$$(26) \quad \alpha_{\text{belt}} = \frac{A_{\text{belt}}}{A_C} = \frac{0.95 \text{ W/K}}{10 \text{ mm} \cdot 50 \text{ mm} \cdot \pi} \approx 605 \frac{\text{W}}{\text{m}^2\text{K}}$$

can be calculated.

This is only the contribution of the belt itself. An additional term arises from the conductance of a thin layer air surrounded by the lamellae:

$$(27) \quad \alpha_{\text{air}} = \frac{\lambda_{\text{air}}}{d} = \frac{0.0261 \text{ W/(mK)}}{0.8 \text{ mm}} \approx 32.6 \frac{\text{W}}{\text{m}^2\text{K}}$$

Together with a $12 \text{ W/(m}^2\text{K)}$ contribution from radiation a total equivalent heat transfer coefficient of $650 \text{ W/(m}^2\text{K)}$ is set for the lamella belts. For the vis-à-vis-surfaces of the bolt and the inner bore of the bushing not in electrical contact from conduction through a thin layer of air and radiation a heat transfer coefficient of $534 \text{ W/(m}^2\text{K)}$ is obtained.

The contact resistance of the outer thread of the bushing is assumed to be $4 \mu\Omega$ from experience. With (6) an equivalent surface transfer conductivity $g_{A,\text{thread}}$ of $0.25 \text{ MS} / (0.095 \cdot 2\pi \cdot 0.034 \text{ m}^2) \approx 12.32 \text{ MS/m}^2$ is obtained. For the heat transfer coefficient, $\alpha_{\text{thread}} = 900 \text{ W/(m}^2\text{K)}$ is estimated, which would be equivalent to a $29 \mu\text{m}$ air layer. Owing to the direct contact, the transfer conditions are probably better.

The electric current imposed to the model is half the exciter current, $3250/2 \text{ A}$.

Results

An example for a resulting temperature distribution is given in Fig. 4 showing a hot spot on the outer thread close to the central insulation layer of the axial lead. The maximum temperatures are calculated according to (23). However, allowable temperature limits according to [1] are not exceeded. The temperature variation inside the metallic structures is nearly negligible. This is due to the high thermal conductivity. Despite the low distance of the threaded bushing to the central insulation wall there is no danger of overheating of any insulation material or contact surfaces.

Fig. 5 shows the contact current density distribution for the three lamella belts and the outer thread of the bushing. The current density is not completely uniform, but there are only slight variations on the surfaces. The average values which can be calculated from an assumed uniform current

density transition are $J_{n,1,2,\text{avg}} \approx 0.345 \text{ A/mm}^2$ and $J_{n,2,3,\text{avg}} \approx 0.0801 \text{ A/mm}^2$. A homogenization of the current density distributions in the contacts due to the relatively high contact resistances can be suspected.

An interesting question is how (23) applies on the surfaces, i.e. is there an internal contact temperature rise due to contact heat or is the contact temperature just the maximum of both side temperatures? Fig. 6 is an answer to this question as it shows the difference between the maximum temperature from (23) and the maximum of the two side temperatures, i.e.

$$(28) \quad \Delta\vartheta_{1,2,\text{max}} = \vartheta_{1,2,\text{max}}|_{(23)} - \max(\vartheta_1, \vartheta_2)$$

In the contact area 1,2 there is a slight internal temperature rise, whereas the maximum temperature in the contact area 2,3 is given by the maximum of both boundary temperatures which in the given case is ϑ_2 .

Fig. 7 shows the temperature difference at the contact surfaces. Interestingly, the lowest temperature drops occur at those areas where the temperature itself becomes maximum according to Fig. 4 and vice versa. Obviously these domains with heat accumulation are also characterized by low heat transfer rates whereas areas far away from the hot spots exhibit higher temperature gradients and heat transfer rates.

In Fig. 8 the contact voltage drops $u_{1,2}$ and $u_{2,3}$ are depicted. Like in the current density distribution given by Fig. 5 there only occur slight inhomogenities. The voltage drops only amount to some millivolts, which is far away from any values dangerous for the contact integrity as they are given by the softening voltage (90 mV) and the melting voltage (370 mV) for silver plated contacts [4].

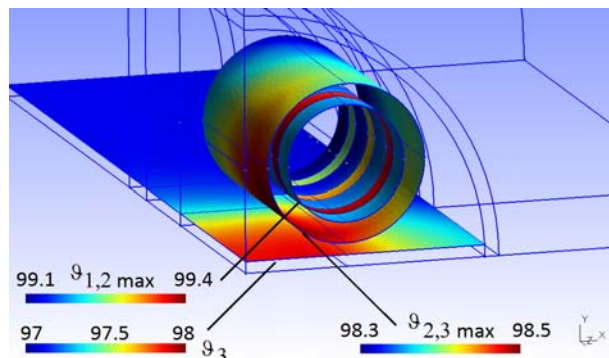


Fig.4. Temperature distribution on contact surfaces and central insulation layer in centigrade.

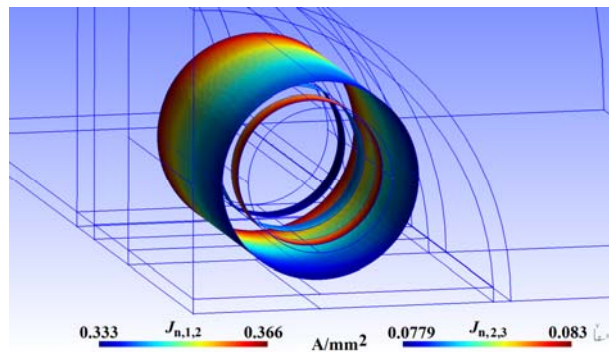


Fig.5. Current density distribution on electrical contact surfaces.

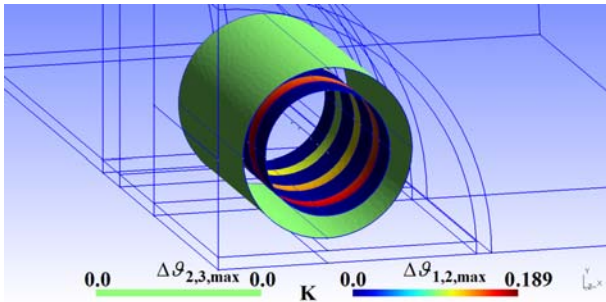


Fig.6. Contact temperature rise in lamella belts and outer thread.

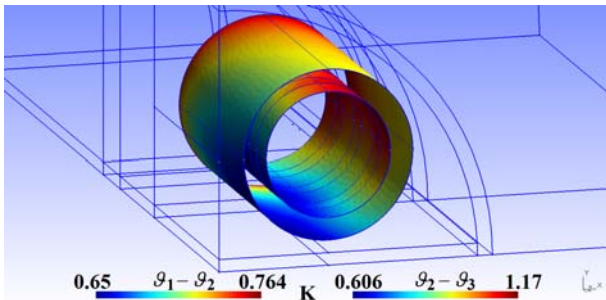


Fig.7. Temperature drop over contact surfaces of lamella belts and intermediate spaces as well as outer thread.

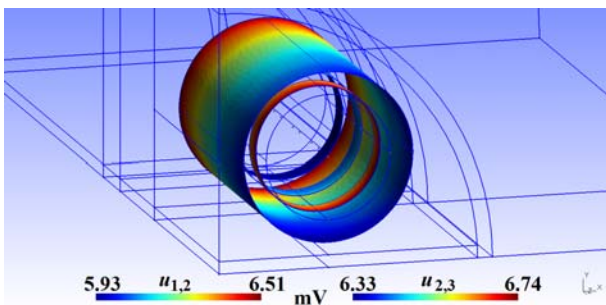


Fig.8. Voltage drop over contact surfaces of lamella belts and outer thread.

Conclusion

A method for the simultaneous computation of a coupled electrical and thermal field problem is presented based on FEM. The contact discontinuities of the electric potential and temperature over surfaces in touch are taken into account by definition of different function spaces in adjacent domains with a suitable formulation for this type of coupled problem.

The method is applied to a service modified turbine generator exciter coupling with bolted and screwed electric contacts in series.

The electrical and thermal results show no critical condition of the arrangement. Contact surface as well as insulation temperatures are in an acceptable range including their hot spot values. The contact voltages are even below the softening values. Thus no harm of the contact integrity has to be expected.

The modification of the coupling under investigation is released based on these results.

Author: Meinolf Klocke, Siemens AG, D 45478 Mülheim a.d. Ruhr, Germany, meinolf.klocke@siemens.com

REFERENCES

- [1] IEC 60137, Ed. 7: Insulated bushings for alternating voltages above 1000 V
- [2] Dular, P.; Geuzaine, C.; Henrotte, F.; Legros, W., A General Environment for the Treatment of Discrete Problems and its Application to the Finite Element Method, *IEEE Trans. Mag.*, Vol. 34, No. 5, p. 3395 – 3398, May 1998
- [3] Runge, B., Dreidimensionale Berechnung der Stillstandserwärmung von Kurzschlußringen und Stäben explosionsgeschützter Asynchronmotoren unter Berücksichtigung des Wärmeübergangswiderstandes zwischen Stab und Blechpaket mittels Finiter-Elemente und Zeitschrittverfahren, PhD thesis, University of Dortmund, 1995
- [4] Rzhia, E. v., Starkstromtechnik, Achte Auflage, Band II, Verlag von Wilhelm Ernst & Sohn, 1960